LBNL-44966

Using an Effective Continuum Model for Flow and Transport in Fractured Rock: The H-12 Flow Comparison

Christine Doughty and Kenzi Karasaki
Earth Sciences Division
E.O. Lawrence Berkeley National Laboratory

December, 1999

This work was supported by Japan Nuclear Fuel Cycle Corporation (JNC) and JGC Corporation. through the U.S. Department of Energy Contract No. DE-AC03-76SF00098.

1. Introduction

The Japan Nuclear Cycle Development Institute (JNC) has initiated a multi-national project to investigate the uncertainties involved in the prediction of flow and transport behavior of a fractured rock mass. In this project, the H-12 flow comparison, several research organizations conduct numerical simulations with the same starting information regarding the fractured rock mass. Subsequently, the results are compared to identify and quantify the uncertainties in the model predictions. We believe that this is potentially a very fruitful exercise. We do not believe, however, that there is much to gain in comparing how computer codes solve algebraic equations. A larger and often overlooked uncertainty lies in the development of the conceptual model. Another source of uncertainty that is tightly related to the development of the conceptual model is in site characterization: the design, execution, and interpretation of the field tests.

In the H-12 flow comparison, most of the specified parameters are only directly meaningful to the discrete fracture network (DFN) modeling approach. These parameters include the fracture transmissivity, fracture aperture and other statistical information on the fracture geometry. We think the geometric data are useful, but we only regard them as soft data. The reasons are as follows: (1) It is virtually impossible to test individual fractures to measure and determine their transmissivity in the field. Therefore, the fracture transmissivity quoted in the literature is invariably inferred from borehole flow tests by making certain assumptions regarding the flow geometry. The measured value is likely to be the effective transmissivity of a collection of interconnected fractures in an unknown volume and of variable directions. (2) Fractures are in general neither planer, circular, nor square. (3) Variability of the hydraulic conductance (transmissivity) within a fracture is likely to be larger than the variability among fractures. (4) Correlations between the parameterized fracture geometry and the hydraulic properties of fractured rock mass may or may not exist.

Our approach to modeling flow and transport in a fractured rock mass is to construct a conceptual model by inverting the field hydrologic test data (hard data) such as the responses during flow tests and pressure interference tests. Unfortunately, our approach is largely incompatible with the specifications given for the H-12 flow comparison. Nevertheless, we hope to make a contribution to this exercise by illustrating how we had to reverse-interpret some of the specified parameters to construct an effective continuum model (ECM), which we regard as a reasonable model given the specifications.

In our model, a stochastic permeability distribution is used to represent the fractured rock block. Individual fractures are not modeled explicitly. The properties of the DFN model specified in the H-12 flow comparison are interpreted as representing conditions observed in the field, and hence serve to constrain the grid design and the parameters used in the ECM. In particular, we generate the stochastic permeability distributions based on an analysis of hydraulic conductivity data from pressure testing at the Kamaishi mine (Oyamada and Takase, 1999, Appendix B). This conductivity data also provides the basis for the fracture transmissivity distribution in the H-12 specifications.

2. H-12 Problem Specification

2.1 Model Region

The region to be modeled is a 200-m by 200-m by 200-m cube of granitic rock containing a 200-m long cylindrical gallery of 2.2 m diameter, which is located in the middle of the volume (Figure 1). The gallery is surrounded by an excavation-damaged zone (EDZ) with a uniform thickness of 0.5 m. Flow is perpendicular to the gallery along the *y*-axis and, thus, a no-flow boundary condition is assumed for all the *x*-*y* and *y*-*z* boundary planes. Heads are assumed uniform on both *x*-*z* boundary planes and the head difference between the two planes is 1.6 m. The surface of the cylindrical gallery is set as a no-flow boundary condition.

2.2 Hydrologic Properties

Fracture Network

Two vertical fracture sets with principal directions aligned with the *x*- and *y*-coordinate axes are considered. Individual fractures deviate in their orientation around the principal directions. The probability density function (pdf) for the fracture orientation θ is given by the Fisher distribution shown in Figure 2. The expression giving $f(\theta)$ is

$$f(\theta) = \frac{\kappa \sin\theta}{4\pi \sinh\kappa} \exp(\kappa \cos\theta),$$

with $\kappa = 10$. Each fracture is regarded as a disk of radius *r*. The pdf for *r*, *f(r)*, follows the truncated power law function shown in Figure 3, with *f(r)* given by

$$f(r) = \frac{\dfrac{b-1}{r_{\min}}\left(\dfrac{r_{\min}}{r}\right)^{b}}{1-\left(\dfrac{r_{\min}}{r_{\max}}\right)^{b-1}},$$

where $r_{\min}$ = 7 m, $r_{\max}$ = 300 m, and b = 3. Fracture centers are located according to a Poisson distribution with frequency chosen to achieve 0.26 fracture/m as the average one-dimensional fracture density (i.e., the average number of fractures intersecting a unit length of a straight line).

Transmissivity of individual fractures, T (m^2/s), follows a lognormal distribution with mean M = -8.99 and standard deviation σ = 1.07 in log units. The fracture aperture, α (m), is assumed to be perfectly correlated with the transmissivity *T*, and the relationship is defined by

$$\alpha = 2\sqrt{T}.$$

Excavation-Damaged Zone

The gallery is surrounded by an EDZ with a uniform thickness of 0.5 m. In previous fracture-network models, the EDZ was represented by a rectangular sleeve around the gallery, consisting

of 4 panels (fractures) of transmissivity $5 \cdot 10^{-10}$ m^2/s. Backfill in the gallery is assumed impermeable.

2.3 Performance Measures

The primary outputs of the H-12 flow comparison are three performance measures:

1. The volumetric flow rate through the central 100-m of the EDZ.

2. The groundwater travel time along paths starting from the gallery and ending at the downgradient boundary of the model.

3. The cumulative F-quotient or weighted travel time from the gallery to the downgradient boundary of the model.

These performance measures are described in more detail in Section 5, where the results are presented.

3. Computer Codes

3.1 Flow Simulator

The numerical simulator TOUGH2 (Pruess, 1987, 1991) is used for the flow calculations. TOUGH2 is a general-purpose code that simulates two-phase flow of air and water in gaseous and liquid phases together with tracer and heat transport through porous or fractured geologic media, which may be strongly heterogeneous. Depending on the design of the grid, TOUGH2 can represent individual fractures or fracture networks explicitly or through an effective continuum formulation, as is done here. The only limitation is that Darcy's law governs fluid flow through both the fractures and rock matrix, with relative permeability and capillary pressure functions used to describe the interactions between liquid and gas phases. TOUGH2 was developed at Berkeley Lab and is widely used in the research community and consulting industry for a variety of problems including environmental remediation, geothermal and petroleum reservoir engineering, and nuclear waste isolation (Pruess, 1995, 1998).

For the present work, we employ a simplified equation of state module known as EOS9 (Wu et al., 1996) that considers only a single component (water) under isothermal conditions (15^{o}C). By maintaining pressure conditions above 1 atm, single-phase liquid conditions prevail. The variable used to describe the state of the system is liquid pressure. Gravity is not included in this study, which makes liquid pressure equivalent to hydraulic head.

TOUGH2 uses the integral-finite-difference method (IFDM) for spatial discretization (Edwards, 1972; Narasimhan and Witherspoon, 1976), which offers greatly increased flexibility in grid design compared to typical finite difference methods. Grid blocks can be of arbitrary shape and size, and can be connected to as many neighboring grid blocks as desired. There need be no reference to a global system of coordinates, or to the dimensionality of a particular flow problem. For a regular lattice of grid blocks the IFDM is equivalent to a block-centered finite difference

scheme, making it possible to simulate one-, two-, or three-dimensional rectangular geometries, or problems with radial, cylindrical, or spherical symmetry, in addition to more complicated irregularly arranged grid blocks.

For the present work, we use a rectangular grid with irregular spacing. Each grid block has a porosity and permeability value assigned to it. Flow is calculated across the interface between two adjacent grid blocks using the harmonic mean of the permeabilities of the two grid blocks.

3.2 Stochastic Permeability Field Generator

The correlated random field generator CRFGEN, developed at Berkeley Lab, is used to create the permeability distributions for the TOUGH2 model. CRFGEN first creates an uncorrelated permeability distribution by drawing permeabilities at random from a specified pdf, which could be a normal distribution, a lognormal distribution, or a user-specified distribution. To create a correlated permeability distribution, the user specifies *x*-, *y*-, and *z*-directional variograms, which describe the desired correlation structure of the permeability field in each direction. Variograms are then constructed for the model permeability distribution and compared with the specified variograms, and an objective function is constructed by summing the squared differences between the model variogram and the specified variogram. The optimization algorithm known as simulated annealing is used to minimize the objective function. At each iteration in the optimization, a trial model permeability distribution is created by exchanging the permeabilities of two randomly chosen grid blocks, new model variograms are determined, and the objective function is recomputed. The Metropolis algorithm (Metropolis et al., 1953) is used to determine whether or not the trial model permeability distribution is accepted.

3.3 Groundwater Travel Time Calculation

The commercial graphics package Tecplot is used to determine groundwater travel times from the flow field calculated by TOUGH2. These travel times consider transport due to advection only; no diffusion or dispersion is included. Tecplot displays streamlines originating from the EDZ. Timing marks along the streamlines enable travel time to the downstream boundary of the model to be determined. To calculate weighted travel time, TOUGH2 has been modified to print out a weighted velocity field, which can be used by Tecplot in an analogous manner.

4. Model Development

4.1 Incorporating Fracture Network Properties

Grid Spacing

The choice of grid spacing for the model of the 200 m fractured rock block is constrained by two opposing theoretical factors. On one hand, we want the grid spacing to be small enough to resolve transport behavior. On the other hand, the H-12 specifications provide a minimum fracture length, 7 m, significantly greater than the average fracture spacing, $\delta = 3.85$ m (note that $1/\delta = 1/3.85 = 0.26$ m^{-1}, the one-dimensional fracture density), implying that the fracture network is well connected. To achieve this in the ECM, we want the grid spacing to be greater than the average fracture spacing, so each grid block will contain several fractures. That is, no grid block will represent intact rock matrix. Complementing

these theoretical issues is the practical desire for as coarse a model as possible, to minimize required computer time for simulations and make the file handling accompanying simulation of multiple realizations convenient.

The base case for the present studies considers a 15 x 15 x 15 grid, making the grid spacing in each direction equal to 200/15 = 13.333 m. A finer grid spacing of 200/21 = 9.52 m was also investigated. It is desirable to use an odd number of grid blocks in each direction, to enable placement of the EDZ in the center of the model.

Grid Orientation

The distribution of fracture orientation given in the H-12 specification shows that fracture orientation is widely distributed in space, peaking at about 20° from the coordinate axis directions (Figure 2), which will lead to a tendency for preferential flow in those directions. It is interesting to note that there are a diminishing number of fracture poles oriented in the principal directions. This is often attributable to sampling bias due to the fact that boreholes and drifts have very little chance to sample fractures whose poles are oriented perpendicular to their axis.

The rectangular grid is aligned along the *x*, *y*, and *z* axes, parallel to the orientations of the fracture sets. TOUGH2 allows for anisotropic permeabilities, as long as the principal directions of the permeability tensor are aligned with the coordinate axes. We do not make use of this feature here because the problem specification does not provide different properties for fractures in the *x*-*z* plane and fractures in the *y*-*z* plane. A rectangular grid with five-point finite differencing, the default choice of TOUGH2, provides some preferential flow in the coordinate axis directions, enabling a qualitative representation of fracture orientation.

Permeability Probability Density Function

We use the hydraulic conductivity data from pressure testing at the Kamaishi mine (Oyamada and Takase, 1999, Appendix B) as the basis for the model permeability pdf. There are a total of 48 conductivity measurements, made from packed-off intervals ranging in length from 0.6 to 5 m in six different boreholes. There are a total of $n_{el} = 15^3 = 3375$ model elements that require a permeability value. We assume that each conductivity measurement, K_i, represents the continuum conductivity of the rock surrounding the borehole interval of length L_i in which the pressure test was done. We assign each K_i measurement to $(L_i/L_{total})n_{el}$ elements chosen at random, where $L_{total} = \Sigma L_i = 132.5$ m. The mean log-conductivity of the resulting model is $M = -8$ (10^{-8} m/s) and the standard deviation is $\sigma = 1.15$, however, the pdf is not lognormal. As shown in Figure 4, it exhibits a bimodal character with peaks around 10^{-9} and 10^{-7} m/s.

TOUGH2 requires intrinsic permeability, *k*, as an input, so we need to use dynamic viscosity, μ, to convert from hydraulic conductivity to intrinsic permeability: $K = k/\mu$. With *K* in m/s and *k* in m^2, the units of μ become m·sec (note that the usual S.I. units for dynamic viscosity μ are Pa·sec, but we use hydraulic head in m instead of pressure in Pascals, requiring a corresponding change in the units of μ). As viscosity is temperature-dependent, we assume a temperature of 15°C and take $\mu = 1.16 \cdot 10^{-7}$ m·sec, yielding a log-mean permeability of about 10^{-15} m^2 = 1 md.

Permeability Correlation Structure

The underlying premise used in determining the permeability correlation structure is that in order for pressure tests at the Kamaishi mine to yield large conductivity values based on steady-state pressure and flow measurements, the zones associated with the large conductivity measurements must be spatially extensive. We therefore use longer correlation lengths for high conductivity values than for lower ones.

The correlation structure is determined in two steps. In the first step, the starting conductivity distribution is a random arrangement of the Kamaishi conductivity pdf. Simulated annealing is conducted to match variograms with a long correlation length (~200 m) in all directions, with identical variograms for the *x* and *y* directions, and a somewhat different variogram for the *z* direction (Figure 5). These variograms do not arise from field data, but were constructed by hand specifically to produce extensive vertical planar features of similar conductivity in the *x-z* plane or in the *y-z* plane. Note that the long-correlation variograms do not exhibit well-developed sills at the variance of the conductivity distribution ($\sigma^2 = 1.32$), indicating that correlations exist over the entire model extent.

The second step uses the output of the first step as the starting conductivity distribution. Simulated annealing is conducted to match variograms with short correlation lengths (~30 m) in all directions (Figure 5), with the restriction that no conductivity value greater than a specified value, K_{cutoff}, is altered, thus preserving the long-correlation high-conductivity structure developed in step 1. We take $K_{cutoff} = 10^{-7}$ m/s. As shown in the conductivity histogram (Figure 4), this is a high cutoff value, beyond both peaks in the histogram, making long-correlation features rare, as suggested by *f(r)* (Figure 3). The standard deviation of the log-conductivity distribution with $K < K_{cutoff}$ is $\sigma = 0.96$, and the associated variance $\sigma^2 = 0.92$ is used for the short-correlation variogram sill.

Porosity

Fracture aperture, α, and average fracture spacing, δ, are used to determine ECM porosity, which is needed to estimate groundwater travel times. The expression for aperture originally given in the H-12 specifications, $\alpha = 2(T)^{1/2}$ is problematic in that it is not dimensionally consistent. We use instead the relationship $\alpha_T = 10\alpha_H$, with α_T the tracer aperture, and α_H the hydraulic aperture determined from the cubic law

$$\alpha_T = 10\alpha_H = 10(12\, T\mu)^{1/3}.$$

Both expressions have been cited as arising from calibration to a tracer test at Kamaishi mine (Uchida and Sawada, 1995), and for the transmissivity value used for the calibration (10^{-7} m/s), both expressions yield similar results. We assume that fracture transmissivity T is related to model permeability k according to $T = \delta k/\mu$ (note that $T = K_f\alpha_H$, where K_f is fracture hydraulic conductivity, yielding the familiar relationship between fracture and continuum properties $k/\mu = K = K_f\alpha_H/\delta$).

We then equate the pore volume in a block of fractured rock to the pore volume in a block of ECM with porosity ϕ. This yields

$\phi = 2\ \alpha_T / \delta = 20(12\delta k)^{1/3}/\delta = 20(12k/\delta^2)^{1/3}$.

The factor of 2 arises because there are two fracture sets, each with aperture α_T and spacing δ. We take $\delta = 0.33$ m, the average spacing of exposed cracks measured in the Kamaishi boreholes in which pressure tests were conducted. Note that in the original H-12 specification a fracture density of 0.26 m^{-1} was given, which is equivalent to a much larger fracture spacing of 3.85 m. Because we base our permeability distribution on the Kamaishi conductivity data, it makes sense to use a consistent value for fracture spacing.

4.2 Excavation-Damaged Zone (EDZ)

Grid Spacing

The grid gets finer around the EDZ in order to resolve it as a rectangular solid with a 3.2 by 3.2-m square cross-section (Figure 6).

Properties

The H-12 specifications give the transmissivity of the EDZ as $T_{EDZ} = 5{\cdot}10^{-10}$ m^2/s. To convert transmissivity to permeability, as required for TOUGH2, we use the thickness of the EDZ grid blocks, $b = 3.2$ m:

$k_{EDZ} = T_{EDZ}\mu/b = 18$ μd.

To determine the porosity of the EDZ blocks, we use the ratio of the volume of the EDZ (calculated based on its annular geometry) to the volume of the grid block representing it, then multiply by an estimate of the porosity of the EDZ material itself (1%):

$\phi_{EDZ} = V_{EDZ}/V_{grid} = \pi(1.6^2\text{-}1.1^2)\ /(3.2)^2\ 0.01 = 0.0041$.

This formulation assumes that the grid blocks representing the gallery within the EDZ are impermeable and have zero porosity.

4.3 Boundary Conditions

Constant pressure boundaries are imposed at the upstream and downstream boundaries of the model by adding planes of small grid blocks at $y = 0$ and $y = 200$ m. To achieve a head difference of $\Delta h = 1.6$ m, we use a pressure difference of $\Delta P = 0.1567$ bars ($P = \rho g h$, where $g = 9.8$ m/s^2 and $\rho = 999.30$ kg/m^3 for 15°C).

5. Model Application

TOUGH2 calculates a steady-state flow field by starting from an arbitrary initial condition and letting the system evolve toward steady state under the influence of the imposed boundary conditions. For the present work, the initial pressure in the model was taken to be the mean of the upstream and downstream boundary pressures. The simulations described below reached

steady state within 30-50 time steps, and each required 1-3 minutes of computer time on a Pentium 120 personal computer. At steady state, three particular performance measures were calculated to enable comparison of results between different research organizations.

5.1 Illustrative Flow Fields

An example of the variograms returned by the first annealing step is shown in Figure 7. Note that only two of the three returned variograms match the specified long-range variograms (Figure 5) better than an uncorrelated medium with flat variograms would. For the given conductivity PDF, this sort of partial match is the best match that can be obtained. The corresponding conductivity distribution is shown in the left column of Figure 8; it corresponds to through-going fractures in the *y*-*z* plane. In general, it is found that about half the realizations produce through-going fractures in the *x*-*z* plane and half produce through-going fractures in the *y*-*z* plane. Occasionally neither fracture set extends all the way across the model. The conductivity distribution returned by the second annealing step is shown in the right column of Figure 8. The corresponding variograms (not shown) do not exhibit any significant structure, indicating that low permeabilities are not correlated over distances greater than the grid spacing (13.3 m).

A total of 20 realizations of the conductivity distribution were created. Each was used for the simulation two times: once in its original orientation, and once with all the *x* and *y* coordinates exchanged (producing a distribution reflected about the line $y = x$). Hence, high-conductivity features in the *x*-*z* plane would become high-conductivity features in the *y*-*z* plane, and vice versa.

5.2 Performance Measure Algorithms

Performance Measure 1 – Average Flow Rate through the EDZ

The volumetric flow rate, q, through the central 100-m section of the EDZ is calculated by summing all flows entering the central 100-m section of the EDZ. The total flow leaving the central portion of the EDZ is also calculated, as a check that steady-state conditions have been achieved. To calculate average Darcy velocity, v_d, the total volumetric flow entering the central portion of the EDZ can be divided by the area of the upstream face of the central portion of the EDZ ($3.2 \cdot 100 = 320$ m^2). Use of Darcy velocity enables comparison of flow through the EDZ and flow through the block as a whole, to enable investigation of the effect of the properties assigned to the EDZ.

Performance Measure 2 – Groundwater Travel Time

Groundwater (or tracer) travel time is calculated by integrating $1/v_T$ along the flow paths from the EDZ to the downstream model boundary, using the commercial graphics package Tecplot. The tracer velocity v_T is calculated by TOUGH2 as $v_T = v_d/\phi = v_d\delta/(2\alpha_T)$, then it is passed on to Tecplot for post-processing. After all the streamlines are plotted, the ones with the fewest and most timing marks are identified by hand as the fastest and slowest flow paths, respectively, and the corresponding arrival times at the downstream boundary are recorded.

Streamlines are initiated close to the downgradient edge of the EDZ. This provides a lower limit on actual travel times, which may include a contribution from time spent moving through the

EDZ. However, since EDZ properties are not well known, we prefer not to include this uncertainty.

Performance Measure 3 – Cumulative F-quotient (Weighted Travel Time)

Weighted travel time is calculated by integrating $2/v_T\alpha_T$ along the flow paths from the EDZ to the downstream model boundary. The fastest and slowest weighted travel times are then determined using the procedure of performance measure 2. The velocity weighting factor, $\alpha_T/2$, approximates the ratio of the flowing water volume to the flow path surface area. It has been proposed as a useful measure when retardation arises from fracture/matrix interactions (Elert et al., 1997). Note that with $\alpha_T \sim T^{1/3}$, the weighted velocity, $v_w = v_T\alpha_T/2$, will be orders of magnitude smaller than the tracer velocity, hence the weighted travel time will be correspondingly greater than the tracer travel time. Note also that the weighted velocity is actually independent of tracer aperture, since we can substitute the expression for tracer velocity $v_T = v_d\delta/(2\alpha_T)$ to yield $v_w = v_d\delta/4$. Since we take δ as a constant average fracture spacing, weighted velocity is simply proportional to Darcy velocity along each flow path.

5.3 Performance Measure Results

Table 1 summarizes the average performance measures for the 40 simulations, along with results for a uniform medium and averages for 15 realizations of an uncorrelated random field based on the Kamaishi conductivity pdf. For the smaller variations that occur for the uncorrelated random field, simulating 15 realizations is sufficient to produce stable averages. The standard deviation is shown in parentheses below each average value.

Table 1. Summary of Performance Measures for the H-12 flow comparison. Table entries are mean values, with standard deviations in parentheses.

Performance Measure	1. Volumetric flow through EDZ (m^3/s)	1a. Darcy flow through whole model (m/s)	2. Fastest tracer travel time (yr)	2a. Slowest tracer travel time (yr)	3. Fastest cumulative F-quotient (yr/m)	3a. Slowest cumulative F-quotient (yr/m)
Correlated random field[a]	**9.52 E-10** (5.48 E-10)	1.69 E-10 (9.49 E-11)	**21.7** (13.2)	170. (67.2)	**1.30 E5** (1.02 E5)	2.46 E6 (1.89 E6)
Uncorrelated random field[a]	1.27 E-9 (5.55 E-10)	1.06 E-10 (3.69 E-12)	27.7 (5.61)	133. (38.1)	1.99 E5 (6.82 E4)	2.72 E6 (2.30 E6)
Uniform medium[b]	2.01 E-9	7.99 E-11	40.9	40.9	5.01E5	5.01E5

[a]log-mean $K = 10^{-8}$ m/s
[b]$K = 10^{-8}$ m/s

The Darcy flow through the model as a whole is greater than Darcy flow through the EDZ (volumetric flow divided by 320 m^2), reflecting a flow diversion that occurs around the EDZ due

to its low permeability. As the possibility for preferential flow increases (going from the uniform medium model to the uncorrelated random field model to the correlated random field model), flow through the EDZ decreases, flow through the model as a whole increases, and travel times decrease. The fact that flow through the EDZ is inversely correlated with flow through the whole model reflects the fact that when through-going fractures are present in the *y*-*z* plane, they are likely to intersect the EDZ at some point along the *x*-axis. At that point, they allow flow to easily bypass the EDZ. Thus, in addition to increasing flow through the model as a whole, extensive *y*-*z* plane fractures serve to lessen flow through the EDZ.

Figure 9 shows performance measures 1, 1a, 2, and 3 for the 40 realizations of the correlated random field. It is apparent that the two sub-populations (those with through-going *y*-*z* plane fractures and those without) produce sharply different behavior: lower flow through the EDZ, higher flow through the model, and shorter travel times when through-going fractures are present. As expected for a bimodal population, the averaging process produces slow convergence, a mean that is not representative of either population, and a large standard deviation.

6. Discussion

Based on the results presented above, we believe that correlated permeability fields are better suited than uncorrelated fields to represent fractured rock systems in which fracture length may greatly exceed grid block dimension. The uncorrelated results are presented above to highlight the differences between the two methods, and provide insights into how connectivity of high and low permeability features affects overall system behavior. Unfortunately, knowing the optimal correlation structure to impose is not possible given the present data set. A key feature of the present work is correlation lengths that are comparable to the overall dimension of the rock block being studied. In such a case, continuous features tend to extend across the entire system, and preferential flow grows in importance relative to the uncorrelated case.

Figure 10 shows an example of the streamlines used to track the movement of tracer between the EDZ and the downgradient edge of the model. A huge variation in travel times among streamlines leaving different parts of the EDZ is apparent.

The algorithm used to determine ECM porosity accounts for the pore space provided by two fracture sets, those in the *y*-*z* plane and those in the *x*-*z* plane. However, for flow that is predominantly in the *y* direction, as shown in Figure 10, it may be more appropriate to only count fractures in the *y*-*z* plane, as this is where most of the flow occurs. This assumption would reduce the effective porosity by a factor of two, and correspondingly reduce the tracer travel times from the EDZ to the downstream model boundary by a factor of two as well. Weighted travel time would not be affected, as weighted velocity does not depend on tracer aperture.

A limited number of realizations were created using a finer resolution (21 x 21 x 21 grid blocks, each 9.5 m on a side, as opposed to the usual model consisting of 15 x 15 x 15 grid blocks, each 13.33 m on a side). Although the higher-resolution conductivity distributions look appealing, preliminary results suggest that they do not produce significantly different results for the performance measures.

7. Comparison to Other Approaches

7.1 Overview of Approaches

Table 2 shows the research organizations participating in the H-12 flow comparison. Most of the modeling approaches use a DFN model. A complete description of the different modeling approaches and their results is given in Oyamada and Ikeda (1999). The H-12 flow comparison was presented in two stages. In the first stage, research groups were requested to solve the specified problem as closely as possible. In the second stage, groups were provided with more of the characterization data from Kamaishi and allowed to modify the problem specifications as desired to better represent those conditions.

The Berkeley Lab results described in the previous sections reflect our Stage 2 calculations. There are two main differences from our Stage 1 calculations. (1) An increase in mean model permeability by a factor of 12, arising from use of the Kamaishi conductivity data and a fracture spacing of $\delta = 0.33$ m instead of the H-12 specification of transmissivity, converted to conductivity using $\delta = 3.85$ m. (2) Use of longer correlation lengths for high permeability values.

Three of the other groups also noted inconsistencies in the H-12 specifications, and made similar changes. AEA increased the mean value of fracture transmissivity by a factor of 14 to obtain a consistent relationship between Kamaishi conductivities, fracture transmissivity, and average fracture density (Hartley and Jackson, 1999). Taisei increased the mean value of fracture transmissivity by a factor of 10, to better match 'virtual injection test' results obtained with their DFN model to pressure test results from the Kamaishi mine (Shimo and Yamamoto, 1999). UCB explicitly coupled the fracture transmissivity and fracture length in their stochastic fracture generation process (Ahn and Lim, 1999).

In the following figures comparing performance measures, both Stage 1 and Stage 2 results are shown for AEA, Taisei, UCB, and LBL. Kyoto University only participated in Stage 1 and QuantiSci made different modifications for Stage 2, which are not directly comparable with the others, so they are not included.

7.2 Performance Measures

Figures 11 – 13 show the three performance measures from each of the research groups and Figure 14 shows a similar plot for the flow rate through the whole model, which most groups also reported. Each plot shows the mean, M, for a number of realizations (squares). If standard deviation σ was reported, the plots also display $M + \sigma$ and $M - \sigma$ (diamonds), as an estimate of the range of values obtained for different realizations. In some cases, $\sigma > M$, making $M - \sigma$ negative. Because negative numbers cannot be displayed on a log scale, and in any event do not make sense for a travel time, they have been replaced by the lower limit of the plotted range. The large variability among realizations is expected for strongly heterogeneous media such as fractured rock. It emphasizes the need to interpret mean results cautiously, as individaul realizations may show significantly different behavior.

Table 2. Research organizations participating in the H-12 flow comparison.

Organization	**Model**	**Features of Model**
AEA Technology	NAPSAC	DFN
Kyoto University[a]	JOINT-OKY	DFN
University of California, Berkeley (UCB)	FFDF	DFN used to determine properties for an ECM
Taisei Corporation	FNET_FLO	DFN
QuantiSci	FRAC-AFFINITY	Hybrid DFN/ECM[b]
Lawrence Berkeley National Laboratory (LBL)	TOUGH2	ECM

[a]Stage 1 only
[b]DFN only for Stage 1

In general, our ECM results fit in well with the DFN results for all the performance measures. The variability between research groups is not much larger than the variability between realizations, indicating an overall consistency between the different modeling approaches. The transitions from Stage 1 to Stage 2 results generally show larger flow rates and shorter travel times, as expected for an overall increase in transmissivity and a coupling between fracture length and transmissivity. Some particular findings are discussed below.

For performance measure 1, flow through the EDZ, the means for the Stage 1 results are within an order of magnitude of each other (Figure 11). Given the σ values of at least half an order of magnitude, this represents good consistency between the various approaches. With the higher fracture transmissivity of Stage 2, one would expect more flow through the model, but with the same low transmissivity in the EDZ, one would expect most of the additional flow to bypass the EDZ, leaving about the same flow through it. This is what the UCB and LBL results show. However, the AEA and Taisei models show an order of magnitude increase in EDZ flow. Apparently these models assume that fractures extend continuously through the EDZ, so bypass flow does not occur.

For performance measures 2 and 3, tracer travel time and weighted travel time, the means for the Stage 1 results vary within a factor of 10 and 30 respectively, and the Stage 2 results show the expected decrease in travel time for higher transmissivity (Figures 12 and 13). Standard deviations may be much larger for travel times than for EDZ flow, reflecting greater variability between realizations for a given model.

For flow through the whole model (Figure 14), the Stage 1 LBL result is significantly too low, reflecting the inability of the model to represent long, high-transmissivity fractures. This deficiency is corrected for Stage 2, in which the LBL result is in line with that of AEA and Taisei.

8. Summary and Conclusions

In the H-12 flow comparison, six research organizations conducted independent numerical simulations of flow and transport in a saturated fractured rock mass, using the same starting information. Subsequently the results were compared to identify and quantify the uncertainties arising in computer modeling.

The Berkeley Lab modeling approach differed markedly from most of the others, by using an effective continuum model rather than a discrete fracture network model. The results of all the models are reasonably consistent, with variability between realizations of a single model being of comparable magnitude to the variability between models.

The ECM is generally far more efficient than the DFN approach, and as such may be more useful for the larger scale of problems typically encountered in the field. All the LBL simulations presented here were done on a laptop computer with a 120 MHz Pentium processor and 40Mb of RAM.

We believe that even more value would be realized from the H-12 flow comparison exercise if each organization were supplied with the "hard data" and allowed to construct their own conceptual model. This is where crucial model uncertainties can arise. Ideally, the design and execution of the field tests for site characterization should not be dictated by a modeling approach selected a priori. Rather, field tests should proceed concurrently with conceptual model development, with information gained from each activity used to improve the other in an iterative fashion.

Acknowledgements

We thank Stefan Finsterle and John Peterson for reviewing this report, and Yuji Ijiri for assistance describing the H-12 problem parameters. This work was supported by Japan Nuclear Fuel Cycle Corporation (JNC) and JGC Corporation through the U.S. Department of Energy Contract No. DE-AC03-76SF00098.

References

Ahn, J. and D. Lim, H-12 flow calculation by FFDF (2^{nd} stage), in Oyamada and Ikeda, JNC TJ1400 99-023, 1999.

Elert, M. et al., Retention mechanisms and the flow wetted surface – implications for safety analysis, SKB Technical Report 97-01, SKB, Sweden, 1997.

Edwards, A.L., TRUMP: A computer program for transient and steady state temperature distributions in multidimensional systems, National Technical Information Service, National Bureau of Standards, Springfield, VA, 1972.

Hartley, L.J. and C.P. Jackson, H-12 flow comparison: Stage 2 using NAPSAC, in Oyamada and Ikeda, JNC TJ1400 99-023, 1999.

Metropolis, N., A. Rosenbluth, M. Rosenbluth, A. Teller, and E. Teller, Equations of state calculations by fast computing machines, Journal of Chemical Physics, 21, 1087-1092, 1953.

Narasimhan, T.N. and P.A. Witherspoon, An integrated finite difference method for analyzing fluid flow in porous media, Water Resources Res., 12(1), 57-64, 1976.

Oyamada, K. and T. Ikeda, Uncertainty analysis on hydrologic modeling in heterogeneous media (CORE Collaborative Study), Japan Nuclear Fuel Cycle Development Institute TJ1400 99-023, 1999.

Oyamada, K. and H. Takase, Specification for the second stage H-12 flow comparison, in Oyamada and Ikeda, JNC TJ1400 99-023, 1999.

Pruess, K., TOUGH user's guide, Rep. LBL-20700, Lawrence Berkeley Laboratory, Berkeley, CA, 1987.

Pruess, K., TOUGH2 – A general-purpose numerical simulator for multiphase fluid and heat flow, Rep. LBL-29400, Lawrence Berkeley Laboratory, Berkeley, CA, 1991.

Pruess, K., Ed., Proceedings of the TOUGH Workshop '95, Rep. LBL-37200, Lawrence Berkeley Laboratory, Berkeley, CA, 1995.

Pruess, K., Ed., Proceedings of the TOUGH Workshop '98, Rep. LBL-41995, Lawrence Berkeley National Laboratory, Berkeley, CA, 1998.

Shimo, M. and H. Yamamoto, Intercomparison of flow calculation for H-12 reference fractured rock: Progress report on Stage 2 calculation using FNET_FLO, in Oyamada and Ikeda, JNC TJ1400 99-023, 1999.

Uchida, M. and Sawada, A., Discrete fracture network modelling of tracer migration experiments at the Kamaishi mine, Mat. Res. Soc. Proc., Vol. 353, 1995.

Wu, Y.S., C.F. Ahlers, P. Fraser, A. Simmons and K. Pruess, Software qualification of selected TOUGH2 modules, Rep. LBNL-39490, Lawrence Berkeley National Laboratory, Berkeley, CA, 1996.

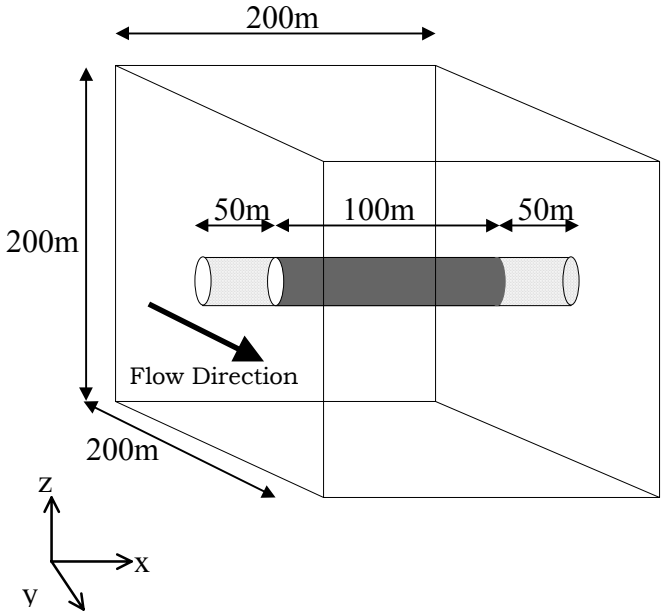

Figure 1. Model region for the H-12 flow comparison (Oyamada and Takase, 1999). The central 100-m of the 200-m long gallery surrounded by the excavation damaged zone is shown shaded (see Performance Measure 1).

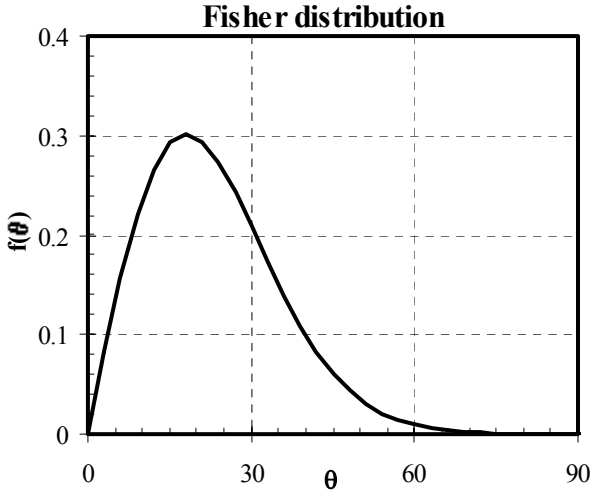

Figure 2. Fisher distribution used to describe the distribution of fracture orientation θ, taken from the H-12 specifications (Oyamada and Takase, 1999).

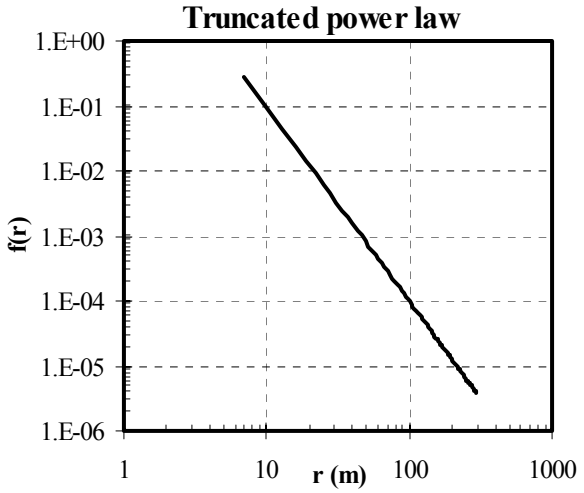

Figure 3. Truncated power law used to describe the distribution of fracture radius, taken from the H-12 specifications (Oyamada and Takase, 1999).

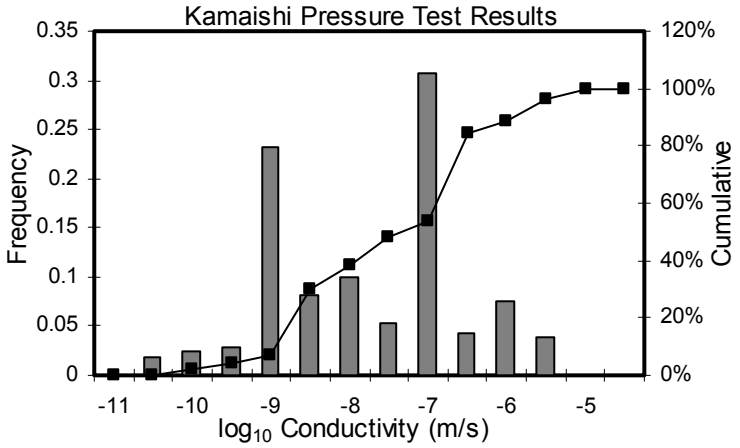

Figure 4. Model log-conductivity histogram, derived from pressure-test data from the Kamaishi mine (Oyamada and Takase, 1999, Appendix B). Note that the bin labels give the upper limit for the log-conductivity for that bin. Thus, the values in the right peak all have $K < 10^{-7}$ m/s.

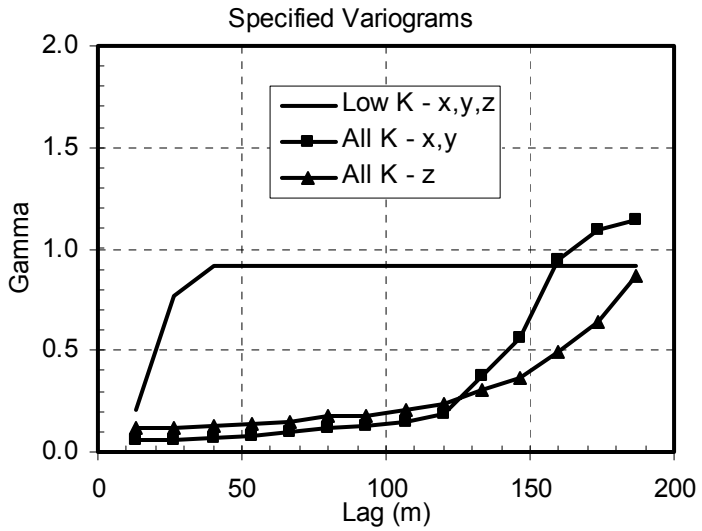

Figure 5. Variograms specified for the generation of the correlated random log-conductivity fields. These variograms do not arise from field data.

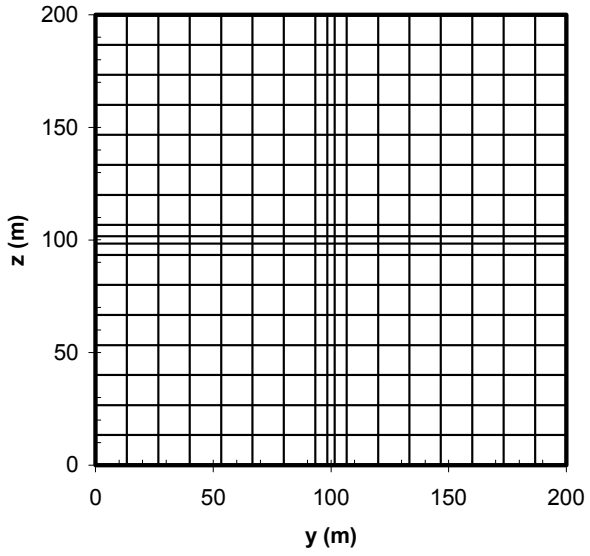

Figure 6. Cross-section of the TOUGH2 grid in the *y*-*z* plane, showing grid spacing that varies from 3.2 m at the EDZ to 13.33 m. The grid spacing in the *x* direction is uniformly 13.33 m.

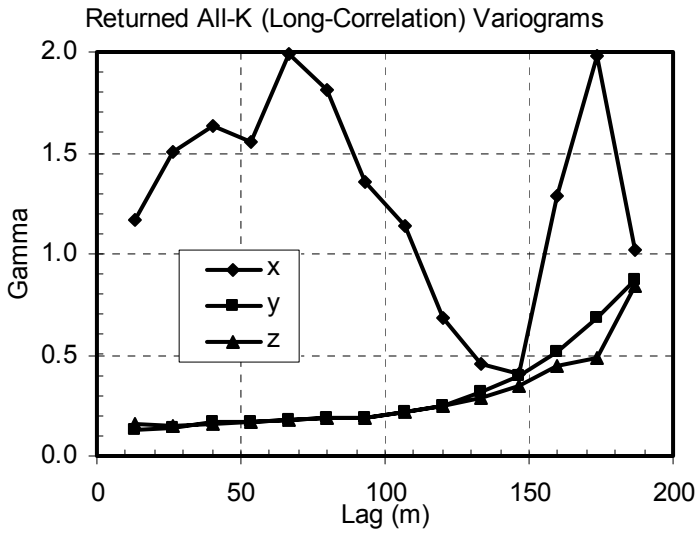

Figure 7. Example of model variograms returned by the first step of annealing, using the specified long-correlation variograms shown in Figure 5. These variograms correspond to through-going fractures in the *y*-*z* plane.

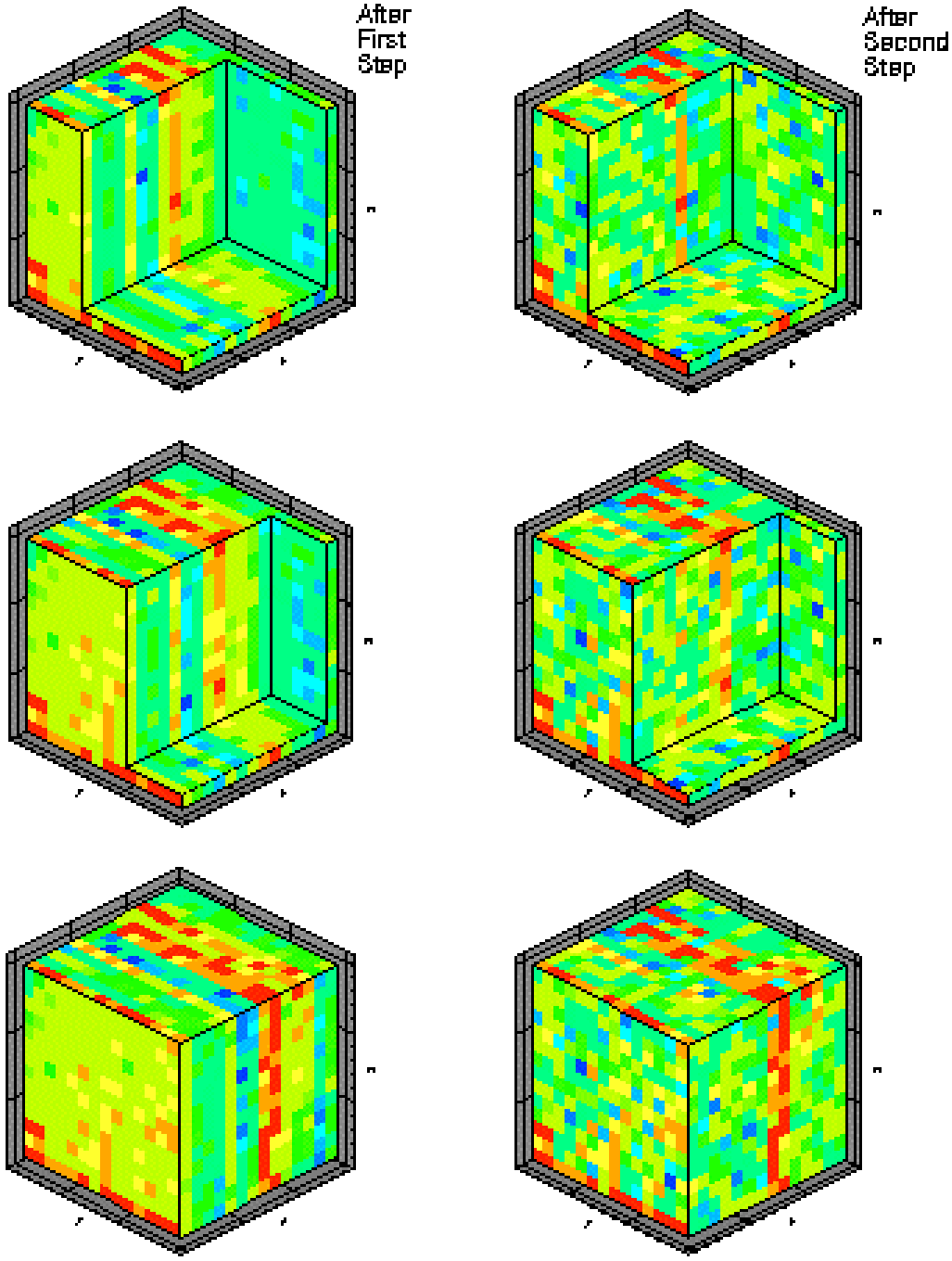

Figure 8. Example conductivity distribution. The left column shows three views of the conductivity distribution resulting from the first step of annealing to the long-correlation variograms. The right column shows the same view of the conductivity distribution resulting from the second step of annealing to the low-*K* short-correlation variograms. High conductivity values are shown in red, low in blue.

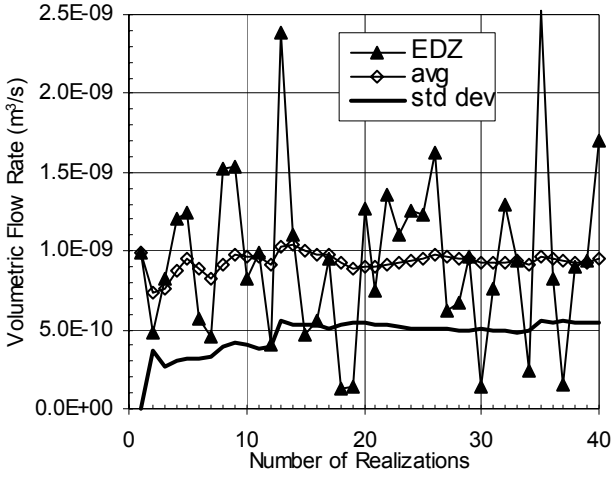
2.5E-09
2.0E-09
1.5E-09
1.0E-09
5.0E-10
0.0E+00
Volumetric Flow Rate (m3/s)
EDZ
avg
std dev
0
10
20
30
40
Number of Realizations

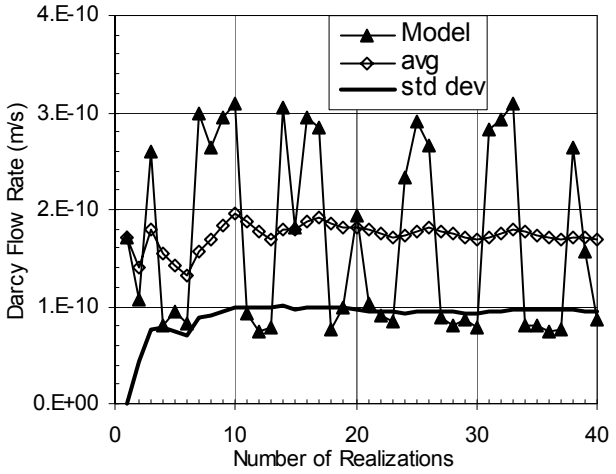
4.E-10
3.E-10
2.E-10
1.E-10
0.E+00
Darcy Flow Rate (m/s)
Model
avg
std dev
0
10
20
30
40
Number of Realizations

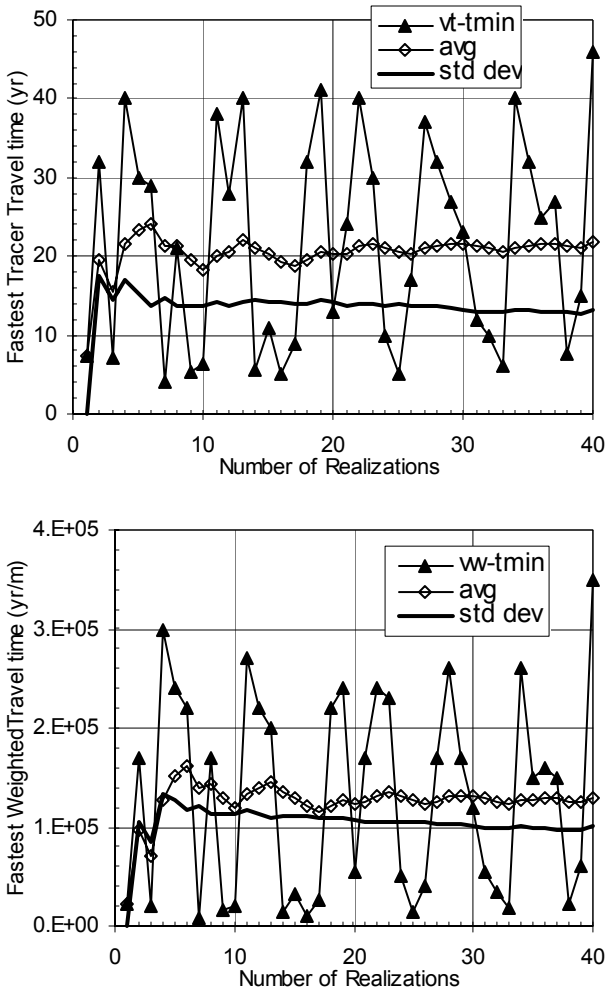

Figure 9. Performance Measures 1 (EDZ flow), 1a (model flow), 2 (fastest tracer travel time), and 3 (fastest weighted travel time) as a function of realization number, for correlated permeability distributions.

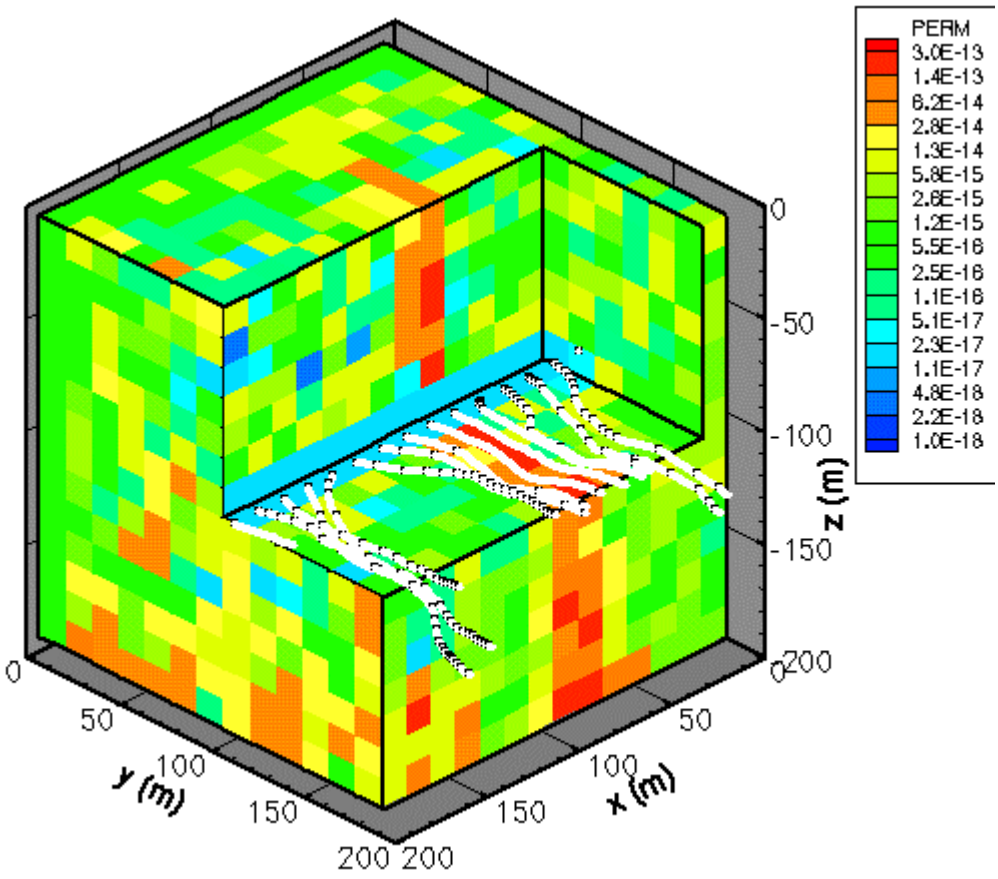

Figure 10. Example of streamlines depicting tracer transport. The black timing marks on each streamline are spaced 10 years apart. Note that the streamlines following the high-permeability feature at about x = 70 m show no timing marks, indicating travel times of less than 10 years.

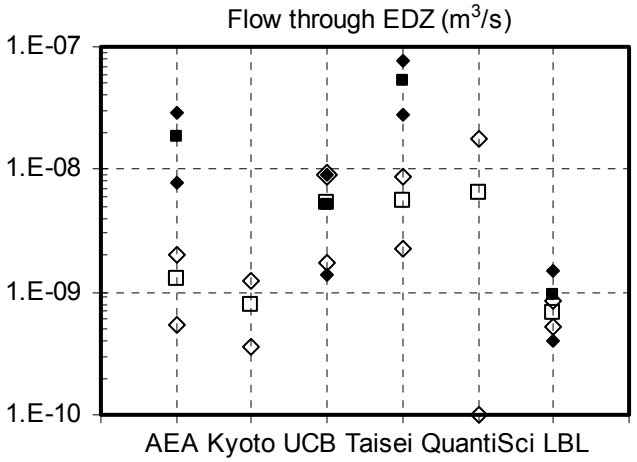

Figure 11. Comparison of Performance Measure 1, flow through the EDZ, for each research group. Square symbols indicate the mean; diamonds give the mean plus or minus one standard deviation. Stage 1 results are shown as open symbols.

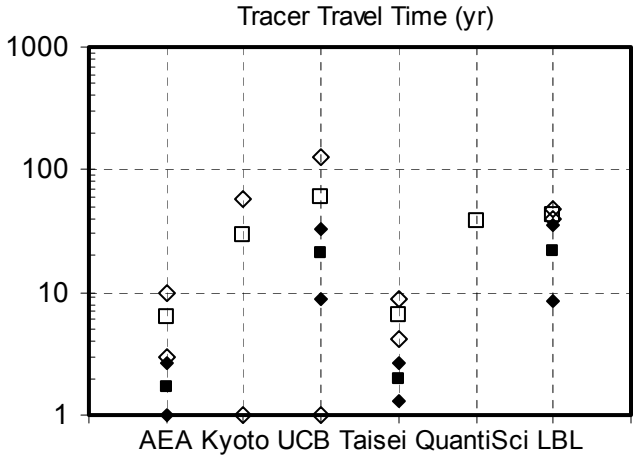

Figure 12. Comparison of Performance Measure 2, fastest tracer travel time, for each research group. Square symbols indicate the mean; diamonds give the mean plus or minus one standard deviation. Stage 1 results are shown as open symbols.

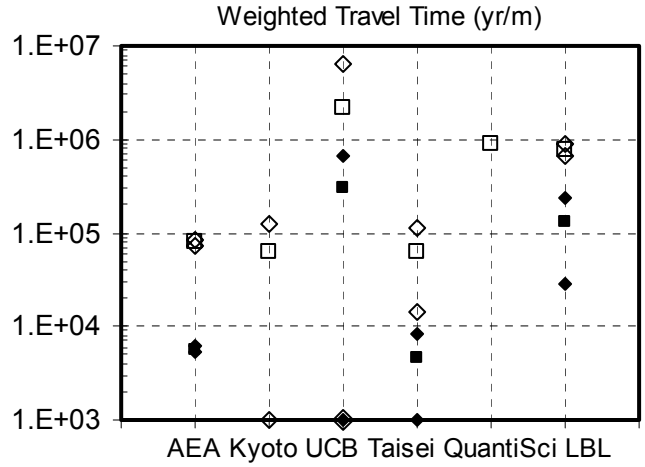

Figure 13. Comparison of Performance Measure 3, fastest weighted travel time, for each research group. Square symbols indicate the mean; diamonds give the mean plus or minus one standard deviation. Stage 1 results are shown as open symbols.

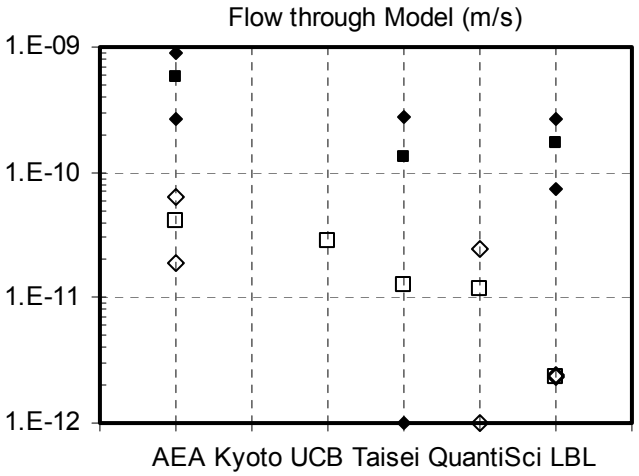

Figure 14. Comparison of flow through the whole model for each research group. Square symbols indicate the mean; diamonds give the mean plus or minus one standard deviation. Stage 1 results are shown as open symbols.